

Space-time Galerkin POD with application in optimal control of semi-linear parabolic partial differential equations

Manuel Baumann¹, Peter Benner², and Jan Heiland^{*2}

¹Delft Institute of Applied Mathematics

²Max Planck Institute for Dynamics of Complex Technical Systems
Magdeburg

November 15, 2016

Abstract

In the context of Galerkin discretizations of a partial differential equation (PDE), the modes of the classical method of Proper Orthogonal Decomposition (POD) can be interpreted as the ansatz and trial functions of a low-dimensional Galerkin scheme. If one also considers a Galerkin method for the time integration, one can similarly define a POD reduction of the temporal component. This has been described earlier but not expanded upon – probably because the reduced time discretization globalizes time which is computationally inefficient. However, in finite-time optimal control systems, time *is* a global variable and there is no disadvantage from using a POD reduced Galerkin scheme in time. In this paper, we provide a newly developed generalized theory for space-time Galerkin POD, prove its optimality in the relevant function spaces, show its application for the optimal control of nonlinear PDEs, and, by means of a numerical example with Burgers' equation, discuss the competitiveness by comparing to standard approaches.

1 Introduction

The method of *Proper Orthogonal Decomposition* (POD) is a standard model reduction tool. For a generic dynamical system

$$\dot{v} = f(t, v), \quad (1)$$

on the time interval $(0, T]$ with a solution v with $v(t) \in \mathbb{R}^N$ and using samples $v(t_j)$, POD provides a set of \hat{n} so-called modes $\hat{v}_1, \dots, \hat{v}_{\hat{n}} \in \mathbb{R}^N$ which optimally parametrize the solution trajectory. As a result, the system (1) can be projected down to a system of reduced spatial dimension \hat{n} that reflects the dynamical behavior of (1) well. If the considered system stems from a *Finite Element* (FEM) discretization of a PDE, then the modes $\hat{v}_i, i = 1, \dots, \hat{n}$ can be interpreted as ansatz functions in the finite element space \mathcal{Y} and the projected system as a particular Galerkin projection of the underlying PDE.

In this paper we provide a theoretical framework and show cases for a space-time Galerkin POD method. The underlying ideas for this generalization of POD have been developed and tested in our earlier works [3, 4].

The first innovation of the proposed generalized POD approach bases on the observation that instead of the discrete time samples $v(t_j)$ one may use the projection of v onto the finite dimensional subspace $\mathcal{S} \cdot \mathcal{Y}$, where \mathcal{S} is a, say, k -dimensional subspace of $L^2(0, T)$. The second innovation is that the projection onto $\mathcal{S} \cdot \mathcal{Y}$ can be interpreted as Galerkin

*Corresponding author's e-mail address: heiland@mpi-magdeburg.mpg.de

discretization in time which can be reduced analogously to the POD reduction of the space dimension. The resulting scheme is a POD reduced space-time Galerkin discretization.

This basic idea of a space-time POD has already been taken up in [20] but not progressed since then. We think that this is due to the fact that temporal POD destructs the causality in time which makes it very inefficient for numerical simulations. In fact, the POD reduced time ansatz functions are global such that the space-time Galerkin system has to be solved as a whole rather than in sequences of time slobes as in standard time-stepping or discontinuous Galerkin schemes [14, 18]. Thus, the reduced space-time scheme cannot compete with, e.g., a spatial POD combined with a standard Runge-Kutta solver. However, in finite-time optimal control problems, the time *is* a global variable and, as we will show by numerical examples, the space-time Galerkin discretization becomes very competitive.

The need and the potential of also reducing the time dimension of a reduced order model have been discussed in [6]. There – similar to our observation that an SVD of a matrix of measurements also reveals compressed time information – it is proposed to use the right singular vectors of a classical snapshot matrix for forecasting.

We want to point out that the method of *Proper Generalized Decomposition* (PGD) is related to the proposed space-time Galerkin POD only in so far as for PGD also space-time (and parameter) tensor bases are used for the modelling; see, e.g., [8]. However, the PGD approach seeks to successively build up the bases by collocation, *greedy algorithms*, and fixed-point iteration, whereas our approach reduces a given basis on the base of measurements. For the same reasons, the connection of the presented approach to other tensor-based low-dimensional approximation schemes [11, 16] as well as to *Reduced Basis* approaches [21] is only marginal.

This paper is organized as follows. At first, we introduce the mathematical framework and rigorously prove the optimality of the reduced space and time bases. Then we illustrate how the reduced bases can be used for low-dimensional space-time Galerkin approximations. In particular, we address how to treat quadratic nonlinearities, how to incorporate initial and terminal values, and how to set up the bases for a general PDE by means of standard approximation schemes. Finally, we illustrate the performance of the space-time Galerkin POD approach for the optimal control of Burgers' equation and compare it to well-established gradient-based methods combined with standard POD.

2 Space-Time Galerkin POD

In this section, we provide the analytical framework for space-time POD. We introduce the considered function spaces and directly prove the optimality of the POD projection in the respective space-time L^2 norm. For a time interval $(0, T)$ and a spatial domain Ω , consider the space-time function space $L^2(0, T; L^2(\Omega))$. Let

$$\mathcal{S} = \text{span}\{\psi_1, \dots, \psi_s\} \subset L^2(0, T) \quad \text{and} \quad \mathcal{Y} = \text{span}\{\nu_1, \dots, \nu_q\} \subset L^2(\Omega)$$

be finite dimensional subspaces of dimension s and q , respectively, and let

$$\mathcal{X} = \mathcal{S} \cdot \mathcal{Y} \subset L^2(0, T; L^2(\Omega)). \quad (2)$$

The space-time L^2 -orthogonal projection $\bar{x} := \Pi_{\mathcal{S} \cdot \mathcal{Y}} x$ of a function $x \in L^2(0, T; L^2(\Omega))$ onto \mathcal{X} is given as

$$\bar{x}(\xi, \tau) = \sum_{j=1}^s \sum_{i=1}^q \mathbf{x}_{i,j} \nu_i(\xi) \psi_j(\tau), \quad (3)$$

where the coefficient $\mathbf{x}_{i,j}$ are the entries of the matrix

$$\mathbf{X} = [\mathbf{x}_{i,j}]_{i=1, \dots, q}^{j=1, \dots, s} := \mathbf{M}_{\mathcal{Y}}^{-1} \begin{bmatrix} ((x, \nu_1 \psi_1))_{\mathcal{S} \cdot \mathcal{Y}} & \dots & ((x, \nu_1 \psi_s))_{\mathcal{S} \cdot \mathcal{Y}} \\ \vdots & \ddots & \vdots \\ ((x, \nu_q \psi_1))_{\mathcal{S} \cdot \mathcal{Y}} & \dots & ((x, \nu_q \psi_s))_{\mathcal{S} \cdot \mathcal{Y}} \end{bmatrix} \mathbf{M}_{\mathcal{S}}^{-1}, \quad (4)$$

where

$$((x, \nu_i \psi_j))_{\mathcal{S} \cdot \mathcal{Y}} := ((x, \nu_i)_{\mathcal{Y}}, \psi_j)_{\mathcal{S}} := \int_0^T \left(\int_{\Omega} x(\xi, \tau) \nu_i(\xi) \, d\xi \right) \psi_j(\tau) \, d\tau.$$

Here, $\mathbf{M}_{\mathcal{Y}}^{-1}$ and $\mathbf{M}_{\mathcal{S}}^{-1}$ are the inverses of the mass matrices with respect to space and time,

$$\mathbf{M}_{\mathcal{Y}} := [(\nu_i, \nu_j)_{\mathcal{Y}}]_{i=1, \dots, q}^{j=1, \dots, q} \quad \text{and} \quad \mathbf{M}_{\mathcal{S}} := [(\psi_i, \psi_j)_{\mathcal{S}}]_{i=1, \dots, s}^{j=1, \dots, s}. \quad (5)$$

Remark 2.1. We will refer to $\mathcal{X} = \mathcal{S} \cdot \mathcal{Y}$ as the measurement space, to the basis functions of \mathcal{Y} and \mathcal{S} as measurement functions, and to \mathbf{X} as the measurement matrix. This means that a function in $L^2(0, T; L^2(\Omega))$ can be measured in \mathcal{X} , e.g. via its projection on \mathcal{X} , and, the other way around, an element \mathbf{X} of \mathcal{X} can be seen as a measurement of some functions in $L^2(0, T; L^2(\Omega))$.

We introduce some representations of the inner product and the norm of functions in $\mathcal{S} \cdot \mathcal{Y}$.

Lemma 2.2 (Space-time discrete L^2 -product). *Let*

$$x^1 = \sum_{j=1}^s \sum_{i=1}^q \mathbf{x}_{i,j}^1 \nu_i \psi_j \in \mathcal{S} \cdot \mathcal{Y}, \quad x^2 = \sum_{j=1}^s \sum_{i=1}^q \mathbf{x}_{i,j}^2 \nu_i \psi_j \in \mathcal{S} \cdot \mathcal{Y},$$

then, with

$$\mathbf{x}^\ell = [\mathbf{x}_{1,1}^\ell, \dots, \mathbf{x}_{q,1}^\ell, \mathbf{x}_{1,2}^\ell, \dots, \mathbf{x}_{q,2}^\ell, \dots, \mathbf{x}_{1,s}^\ell, \dots, \mathbf{x}_{q,s}^\ell]^\top =: \text{vec}(\mathbf{X}^\ell), \quad \ell = 1, 2,$$

the inner product in $\mathcal{S} \cdot \mathcal{Y}$ is given as

$$((x^1, x^2))_{\mathcal{S} \cdot \mathcal{Y}} = \int_0^T \int_{\Omega} x^1 x^2 \, d\xi \, d\tau = (\mathbf{x}^1)^\top (\mathbf{M}_{\mathcal{S}} \otimes \mathbf{M}_{\mathcal{Y}}) \mathbf{x}^2 \quad (6)$$

and the induced norm as

$$\|x^\ell\|_{\mathcal{S} \cdot \mathcal{Y}}^2 := ((x^\ell, x^\ell))_{\mathcal{S} \cdot \mathcal{Y}} = \|\mathbf{x}^\ell\|_{\mathbf{M}_{\mathcal{S}} \otimes \mathbf{M}_{\mathcal{Y}}}^2 = \|\mathbf{M}_{\mathcal{Y}}^{1/2} \mathbf{X}^\ell \mathbf{M}_{\mathcal{S}}^{1/2}\|_F^2, \quad \ell = 1, 2, \quad (7)$$

where $\|\cdot\|_{\mathbf{M}_{\mathcal{S}} \otimes \mathbf{M}_{\mathcal{Y}}}$ denotes the Euclidean vector norm weighted by $\mathbf{M}_{\mathcal{S}} \otimes \mathbf{M}_{\mathcal{Y}}$.

Proof. Straight-forward calculations. \square

Remark 2.3. In practical applications, one uses a *Cholesky*-factorization of the mass matrices (5) rather than the square-root.

Corollary 2.4. *Let $\mathbf{M}_{\mathcal{S}} = \mathbf{L}_{\mathcal{S}} \mathbf{L}_{\mathcal{S}}^\top$ and $\mathbf{M}_{\mathcal{Y}} = \mathbf{L}_{\mathcal{Y}} \mathbf{L}_{\mathcal{Y}}^\top$ be given in factored form. Then, for a given $x \in \mathcal{S} \cdot \mathcal{Y}$ with its coefficient matrix \mathbf{X} and vector $\mathbf{x} = \text{vec}(\mathbf{X})$ it holds that*

$$\|x\|_{\mathcal{S} \cdot \mathcal{Y}}^2 = \|\mathbf{x}\|_{\mathbf{M}_{\mathcal{S}} \otimes \mathbf{M}_{\mathcal{Y}}}^2 = \|\mathbf{L}_{\mathcal{Y}}^\top \mathbf{X} \mathbf{L}_{\mathcal{S}}\|_F^2. \quad (8)$$

Proof.

$$\begin{aligned} \|\mathbf{x}\|_{\mathbf{M}_{\mathcal{S}} \otimes \mathbf{M}_{\mathcal{Y}}}^2 &= \mathbf{x}^\top (\mathbf{M}_{\mathcal{S}} \otimes \mathbf{M}_{\mathcal{Y}}) \mathbf{x} = \mathbf{x}^\top (\mathbf{L}_{\mathcal{S}} \otimes \mathbf{L}_{\mathcal{Y}}) \cdot (\mathbf{L}_{\mathcal{S}}^\top \otimes \mathbf{L}_{\mathcal{Y}}^\top) \mathbf{x} \\ &= \|(\mathbf{L}_{\mathcal{S}}^\top \otimes \mathbf{L}_{\mathcal{Y}}^\top) \mathbf{x}\|_2^2 = \|\text{vec}(\mathbf{L}_{\mathcal{Y}}^\top \mathbf{X} \mathbf{L}_{\mathcal{S}})\|_2^2 = \|\mathbf{L}_{\mathcal{Y}}^\top \mathbf{X} \mathbf{L}_{\mathcal{S}}\|_F^2, \end{aligned}$$

as it follows from basic properties and relations between the Kronecker product, the vectorization operator, and the Frobenius norm. \square

From now on, we will always consider the factorized form. In theory, one can always replace the factors by the square roots of the respective mass matrices.

Next, we will consider a given function $x \in \mathcal{S} \cdot \mathcal{Y}$ and determine low-dimensional subspaces of \mathcal{Y} and \mathcal{S} that can provide low-dimensional approximations to x in a norm-optimal way.

Lemma 2.5 (Optimal low-rank bases in space). *Given $x \in \mathcal{S} \cdot \mathcal{Y}$ and the associated matrix of coefficients \mathbf{X} . The best-approximating \hat{q} -dimensional subspace $\hat{\mathcal{Y}}$ in the sense that $\|x - \Pi_{\mathcal{S}, \hat{\mathcal{Y}}} x\|_{\mathcal{S}, \mathcal{Y}}$ is minimal over all subspaces of \mathcal{Y} of dimension \hat{q} is given as $\text{span}\{\hat{\nu}_i\}_{i=1, \dots, \hat{q}}$, where*

$$\begin{bmatrix} \hat{\nu}_1 \\ \hat{\nu}_2 \\ \vdots \\ \hat{\nu}_{\hat{q}} \end{bmatrix} = V_{\hat{q}}^T \mathbf{L}_{\mathcal{Y}}^{-1} \begin{bmatrix} \nu_1 \\ \nu_2 \\ \vdots \\ \nu_q \end{bmatrix}, \quad (9)$$

where $V_{\hat{q}}$ is the matrix of the \hat{q} leading left singular vectors of the matrix

$$\mathbf{L}_{\mathcal{Y}}^T \mathbf{X} \mathbf{L}_{\mathcal{S}}.$$

Proof. For the time dimension at fixed index j , we consider

$$y := \sum_{i=1}^q \mathbf{x}_{i,j} \nu_i = [\mathbf{x}_{1,j} \quad \dots \quad \mathbf{x}_{q,j}] \begin{bmatrix} \nu_1 \\ \vdots \\ \nu_q \end{bmatrix} \in \mathcal{Y}.$$

Next, we determine the orthogonal projection of y onto $\hat{\mathcal{Y}}$. Therefore, we write y as a function in $\hat{\mathcal{Y}}$ and a reminder \hat{R} in the orthogonal complement:

$$y = [\mathbf{x}_{1,j} \quad \dots \quad \mathbf{x}_{q,j}] \begin{bmatrix} \nu_1 \\ \vdots \\ \nu_q \end{bmatrix} = [\beta_1 \quad \dots \quad \beta_{\hat{q}}] \begin{bmatrix} \hat{\nu}_1 \\ \vdots \\ \hat{\nu}_{\hat{q}} \end{bmatrix} + \hat{R}.$$

We determine the coefficients β_k , $k = 1, \dots, \hat{q}$ by testing against the basis functions of $\hat{\mathcal{Y}}$. By mutual orthogonality of $\hat{\nu}_i$, $i = 1, \dots, \hat{q}$ and their orthogonality against \hat{R} , it follows that

$$\begin{aligned} \beta_k &= \left(\sum_{i=1}^{\hat{q}} \beta_i \hat{\nu}_i, \hat{\nu}_k \right)_{\mathcal{Y}} = \left(\hat{R} + \sum_{i=1}^{\hat{q}} \beta_i \hat{\nu}_i, \hat{\nu}_k \right)_{\mathcal{Y}} = \left(\sum_{i=1}^q \mathbf{x}_{i,j} \nu_i, \hat{\nu}_k \right)_{\mathcal{Y}} \\ &\stackrel{(*)}{=} [\mathbf{x}_{1,j} \quad \dots \quad \mathbf{x}_{q,j}] \mathbf{M}_{\mathcal{Y}} \mathbf{L}_{\mathcal{Y}}^{-T} V_{\hat{q},k} \\ &= [\mathbf{x}_{1,j} \quad \dots \quad \mathbf{x}_{q,j}] \mathbf{L}_{\mathcal{Y}} V_{\hat{q},k}, \end{aligned}$$

where in $\stackrel{(*)}{=}$ we have used that $\hat{\nu}_k = [\nu_1 \quad \dots \quad \nu_q] \mathbf{L}_{\mathcal{Y}}^{-T} V_{\hat{q},k}$ and where $V_{\hat{q},k}$ is the k -th column of $V_{\hat{q}}$ in (9). Thus, we find that the coefficients of the orthogonal projection of y onto $\hat{\mathcal{Y}}$ in the bases of $\hat{\mathcal{Y}}$ and \mathcal{Y} are given through

$$\begin{aligned} \hat{y} &= \sum_{i=1}^{\hat{q}} \beta_i \hat{\nu}_i = [\beta_1 \quad \dots \quad \beta_{\hat{q}}] \begin{bmatrix} \hat{\nu}_1 \\ \vdots \\ \hat{\nu}_{\hat{q}} \end{bmatrix} = [\mathbf{x}_{1,j} \quad \dots \quad \mathbf{x}_{q,j}] \mathbf{L}_{\mathcal{Y}} V_{\hat{q}} \begin{bmatrix} \hat{\nu}_1 \\ \vdots \\ \hat{\nu}_{\hat{q}} \end{bmatrix} \\ &= [\mathbf{x}_{1,j} \quad \dots \quad \mathbf{x}_{q,j}] \mathbf{L}_{\mathcal{Y}} V_{\hat{q}} V_{\hat{q}}^T \mathbf{L}_{\mathcal{Y}}^{-1} \begin{bmatrix} \nu_1 \\ \vdots \\ \nu_q \end{bmatrix} \\ &=: [\hat{\mathbf{x}}_{1,j} \quad \dots \quad \hat{\mathbf{x}}_{q,j}] \begin{bmatrix} \nu_1 \\ \vdots \\ \nu_q \end{bmatrix}. \end{aligned}$$

Noting that $[\mathbf{x}_{1,j} \quad \dots \quad \mathbf{x}_{q,j}]^T$ makes up the j -th column of the matrix \mathbf{X} associated with x , we conclude that the matrix $\hat{\mathbf{X}}$ of coefficients associated with $\Pi_{\mathcal{S}, \hat{\mathcal{Y}}} x$ is given as

$$\hat{\mathbf{X}} = \mathbf{L}_{\mathcal{Y}}^{-T} V_{\hat{q}} V_{\hat{q}}^T \mathbf{L}_{\mathcal{Y}}^T \mathbf{X}$$

and, by Corollary 2.4, we have that

$$\begin{aligned} \|x - \Pi_{\mathcal{S}, \mathcal{Y}} x\|_{\mathcal{S}, \mathcal{Y}} &= \|\mathbf{L}_{\mathcal{Y}}^{\top} \mathbf{X} \mathbf{L}_{\mathcal{S}} - \mathbf{L}_{\mathcal{Y}}^{\top} \hat{\mathbf{X}} \mathbf{L}_{\mathcal{S}}\|_F = \|\mathbf{L}_{\mathcal{Y}}^{\top} [\mathbf{X} - \hat{\mathbf{X}}] \mathbf{L}_{\mathcal{S}}\|_F \\ &= \|\mathbf{L}_{\mathcal{Y}}^{\top} \mathbf{X} \mathbf{L}_{\mathcal{S}} - V_{\hat{q}} V_{\hat{q}}^{\top} \mathbf{L}_{\mathcal{Y}}^{\top} \mathbf{X} \mathbf{L}_{\mathcal{S}}\|_F \end{aligned}$$

which is minimized over all $V_{\hat{q}} \in \mathbb{R}^{q, \hat{q}}$ matrices by taking $V_{\hat{q}}$ as the matrix of the \hat{q} leading left singular vectors of $\mathbf{L}_{\mathcal{Y}}^{\top} \mathbf{X} \mathbf{L}_{\mathcal{S}}$. \square

The same arguments apply to the transpose of \mathbf{X} :

Lemma 2.6 (Optimal low-rank bases in time). *Given $x \in \mathcal{S} \cdot \mathcal{Y}$ and the associated matrix of coefficients \mathbf{X} . The best-approximating \hat{s} -dimensional subspace $\hat{\mathcal{S}}$ in the sense that $\|x - \Pi_{\hat{\mathcal{S}}, \mathcal{Y}} x\|_{\mathcal{S}, \mathcal{Y}}$ is minimal over all subspaces of \mathcal{S} of dimension \hat{s} is given as $\text{span}\{\hat{\psi}_j\}_{j=1, \dots, \hat{s}}$, where*

$$\begin{bmatrix} \hat{\psi}_1 \\ \hat{\psi}_2 \\ \vdots \\ \hat{\psi}_{\hat{s}} \end{bmatrix} = U_{\hat{s}}^{\top} \mathbf{L}_{\mathcal{S}}^{-1} \begin{bmatrix} \psi_1 \\ \psi_2 \\ \vdots \\ \psi_s \end{bmatrix}, \quad (10)$$

where $U_{\hat{s}}$ is the matrix of the \hat{s} leading right singular vectors of

$$\mathbf{L}_{\mathcal{Y}}^{\top} \mathbf{X} \mathbf{L}_{\mathcal{S}}.$$

Remark 2.7. The approximation results Lemma 2.5 and Lemma 2.6 hold in the space-time L^2 norm, which is the appropriate norm for the considered functions and which is not part of the standard POD approach. However, the need for the right norms have been accounted for through the use of weighted inner products or weighted sums. If one lets \mathcal{S} degenerate to a set of Dirac deltas, then Lemma 2.5 reduces to the optimality result [19, Thm. 1.8] for the standard POD approximation in the case that the inner product is weighted with the FEM mass matrix. If one chooses \mathcal{S} such that the induced time Galerkin scheme resembles a time discretization by the trapezoidal rule (in fact, for any Runge-Kutta scheme and choice of discretization points there exists a corresponding (discontinuous) Galerkin scheme), then Lemma 2.5 reduces to the optimality conditions for the *continuous POD* approach given in [19, Sec. 1.3].

Remark 2.8. The idea of generalized measurements also works as a generalization of POD for model order reduction in space. Consider the dynamical system (1), and define $\mathbf{X}_{\mathcal{S}} := [(v_i, \psi_j)_{\mathcal{S}}]_{i=1, \dots, q}^{j=1, \dots, s}$, where v_i is the i -th component of the vector-valued solution. Then the leading left singular vectors of the matrix $\mathbf{X}_{\mathcal{S}} \mathbf{L}_{\mathcal{S}}^{-1}$ are generalized POD modes and a projection of (1) onto the space spanned by those modes yields a POD-reduced dynamical system as we have previously described it under the term *gmPOD* in [4].

3 Space-Time Galerkin Schemes

In this section, we briefly describe how to formulate a general space-time Galerkin approximation to a generic PDE. This regression is then followed by the discussion of low-rank space-time Galerkin schemes on the base of POD reductions of standard Galerkin bases.

Let $\{\hat{\psi}_1, \dots, \hat{\psi}_{\hat{s}}\} \subset H^1(0, T)$ and $\{\hat{v}_1, \dots, \hat{v}_{\hat{q}}\} \subset H_0^1(\Omega)$ be the POD bases in space and time, respectively. Then, a space-time Galerkin approximation of the generic equation system

$$\dot{v} - \Delta v + N(v) = f \quad \text{on } (0, T] \times \Omega, \quad (11a)$$

$$v|_{\partial\Omega} = 0 \quad \text{on } (0, T], \quad (11b)$$

$$v|_{t=0} = v_0 \quad \text{on } \Omega, \quad (11c)$$

is given as follows:

The approximate solution \hat{v} is assumed in the product space $\hat{\mathcal{S}} \cdot \hat{\mathcal{Y}} := \text{span}\{\hat{\psi}_j \hat{\nu}_i\}_{i=1, \dots, \hat{s}; j=1, \dots, \hat{q}}$. We introduce the formal vectors of the coefficient functions

$$\hat{\Upsilon} := \begin{bmatrix} \hat{\nu}_1 \\ \vdots \\ \hat{\nu}_{\hat{q}} \end{bmatrix} \quad \text{and} \quad \hat{\Psi} := \begin{bmatrix} \hat{\psi}_1 \\ \vdots \\ \hat{\psi}_{\hat{s}} \end{bmatrix}$$

and write \hat{v} as

$$[\hat{\psi}_1 \quad \dots \quad \hat{\psi}_{\hat{q}}] \otimes [\hat{\nu}_1 \quad \dots \quad \hat{\nu}_{\hat{s}}] \hat{\mathbf{v}} = [\hat{\Psi}^\top \otimes \hat{\Upsilon}^\top] \hat{\mathbf{v}}, \quad (12)$$

where $\hat{\mathbf{v}} \in \mathbb{R}^{\hat{s}\hat{q}}$ is the vector of coefficients. We determine the coefficients by requiring them to satisfy the Galerkin projection of (11a) for every basis function $\hat{\nu}_i \hat{\psi}_j$, $i = 1, \dots, \hat{q}$, $j = 1, \dots, \hat{s}$

$$\int_0^T \int_{\Omega} \hat{\nu}_i \hat{\psi}_j \dot{\hat{v}} + \hat{\psi}_j \nabla \hat{\nu}_i \nabla \hat{v} + \hat{\nu}_i \hat{\psi}_j N(\hat{v}) \, dx \, dt = \int_0^T \int_{\Omega} \hat{\nu}_i \hat{\psi}_j f \, dx \, dt.$$

The latter equations combined give a possibly nonlinear equation system for the vector $\hat{\mathbf{v}}$ of coefficients, which is assembled as follows: For the term with the time derivative we compute

$$\begin{aligned} \int_0^T \int_{\Omega} [\hat{\Psi} \otimes \hat{\Upsilon}] \frac{\partial \hat{v}}{\partial t} \, dx \, dt &= \int_0^T \int_{\Omega} [\hat{\Psi} \otimes \hat{\Upsilon}] \left[\frac{\partial \hat{\Psi}^\top}{\partial t} \otimes \hat{\Upsilon}^\top \right] \hat{\mathbf{v}} \, dx \, dt \\ &= \int_0^T \int_{\Omega} \left[\hat{\Psi} \frac{\partial \hat{\Psi}^\top}{\partial t} \otimes \hat{\Upsilon} \hat{\Upsilon}^\top \right] \, dx \, dt \hat{\mathbf{v}} \\ &= \left[\int_0^T \hat{\Psi} \frac{\partial \hat{\Psi}^\top}{\partial t} \, dt \otimes \int_{\Omega} \hat{\Upsilon} \hat{\Upsilon}^\top \, dx \right] \hat{\mathbf{v}} =: [dM_{\hat{\mathcal{S}}} \otimes M_{\hat{\mathcal{Y}}}] \hat{\mathbf{v}}. \end{aligned}$$

By the same principles, for the term with the spatial derivatives, we obtain

$$\begin{aligned} \int_0^T \int_{\Omega} [\hat{\Psi} \otimes \nabla \hat{\Upsilon}] \nabla \hat{v} \, dx \, dt &= \int_0^T \int_{\Omega} [\hat{\Psi} \otimes \nabla \hat{\Upsilon}] [\hat{\Psi}^\top \otimes \nabla \hat{\Upsilon}^\top] \hat{\mathbf{v}} \, dx \, dt \\ &= \left[\int_0^T \hat{\Psi} \hat{\Psi}^\top \, dt \otimes \int_{\Omega} \nabla \hat{\Upsilon} \nabla \hat{\Upsilon}^\top \, dx \right] \hat{\mathbf{v}} =: [M_{\hat{\mathcal{S}}} \otimes K_{\hat{\mathcal{Y}}}] \hat{\mathbf{v}}. \end{aligned}$$

Note that in higher spatial dimensions $\nabla \hat{v}$ as well as $\nabla \hat{\nu}_i$ is a vector and, thus, in the preceding derivation, $\nabla \hat{\Upsilon}$ has to be interpreted properly.

Summing up, we can write the overall system as

$$[dM_{\hat{\mathcal{S}}} \otimes M_{\hat{\mathcal{Y}}} + M_{\hat{\mathcal{S}}} \otimes K_{\hat{\mathcal{Y}}}] \hat{\mathbf{v}} + H_{\hat{\mathcal{S}}\hat{\mathcal{Y}}}(\hat{\mathbf{v}}) = f_{\hat{\mathcal{S}}\hat{\mathcal{Y}}}, \quad (13)$$

where

$$M_{\hat{\mathcal{S}}} := [(\hat{\nu}_i, \hat{\nu}_j)]_{i,j=1, \dots, \hat{s}}, \quad (14a)$$

$$dM_{\hat{\mathcal{S}}} := [(\dot{\hat{\nu}}_i, \dot{\hat{\nu}}_j)]_{i,j=1, \dots, \hat{s}}, \quad (14b)$$

$$M_{\hat{\mathcal{Y}}} := [(\hat{\psi}_l, \hat{\psi}_k)]_{l,k=1, \dots, \hat{q}}, \quad (14c)$$

$$K_{\hat{\mathcal{Y}}} := [(\nabla \hat{\psi}_l, \nabla \hat{\psi}_k)]_{l,k=1, \dots, \hat{q}}, \quad (14d)$$

$$H_{\hat{\mathcal{S}}\hat{\mathcal{Y}}}(\hat{\mathbf{v}}) := [((\hat{\nu}_i \hat{\psi}_l, N(\hat{v})))]_{i=1, \dots, \hat{s}; l=1, \dots, \hat{q}}, \quad (14e)$$

and

$$f_{\hat{\mathcal{S}}\hat{\mathcal{Y}}} := [((\hat{\nu}_i \hat{\psi}_l, f))]_{i=1, \dots, \hat{s}; l=1, \dots, \hat{q}}, \quad (14f)$$

are the Galerkin projections of the system operators and the source term assembled in the corresponding inner products.

Remark 3.1. In the space-time Galerkin POD context, the reduced bases are projections of standard finite element bases. Concretely, by virtue of Lemma 2.5 and Lemma 2.6 one has that

$$\hat{\Psi} = U_{\hat{s}}^T \mathbf{L}_{\mathcal{S}}^{-1} \Psi \quad \text{and} \quad \hat{\Upsilon} = V_{\hat{q}}^T \mathbf{L}_{\mathcal{Y}}^{-1} \Upsilon,$$

where the columns of $U_{\hat{s}}$ and $V_{\hat{q}}$ are orthonormal and where $\mathbf{L}_{\mathcal{S}}$ and $\mathbf{L}_{\mathcal{Y}}$ are factors of the mass matrices associated with Ψ and Υ . Accordingly the coefficients in (14) are given as

$$M_{\hat{\mathcal{S}}} := U_{\hat{s}}^T \mathbf{L}_{\mathcal{S}}^{-1} \left[\int_0^T \Psi \Psi^T ds \right] \mathbf{L}_{\mathcal{S}}^{-T} U_{\hat{s}} = U_{\hat{s}}^T \mathbf{L}_{\mathcal{S}}^{-1} M_{\mathcal{S}} \mathbf{L}_{\mathcal{S}}^{-T} U_{\hat{s}} = I_{\hat{s}}, \quad (15a)$$

$$dM_{\hat{\mathcal{S}}} := U_{\hat{s}}^T \mathbf{L}_{\mathcal{S}}^{-1} \left[\int_0^T \dot{\Psi} \dot{\Psi}^T ds \right] \mathbf{L}_{\mathcal{S}}^{-T} U_{\hat{s}}, \quad (15b)$$

$$M_{\hat{\mathcal{Y}}} := V_{\hat{q}}^T \mathbf{L}_{\mathcal{Y}}^{-1} \left[\int_{\Omega} \Upsilon \Upsilon^T dx \right] \mathbf{L}_{\mathcal{Y}}^{-T} V_{\hat{q}} = V_{\hat{q}}^T \mathbf{L}_{\mathcal{Y}}^{-1} M_{\mathcal{Y}} \mathbf{L}_{\mathcal{Y}}^{-T} V_{\hat{q}} = I_{\hat{q}}, \quad (15c)$$

$$K_{\hat{\mathcal{Y}}} := V_{\hat{q}}^T \mathbf{L}_{\mathcal{Y}}^{-1} \left[\int_{\Omega} \nabla \Upsilon \nabla \Upsilon^T dx \right] \mathbf{L}_{\mathcal{Y}}^{-T} V_{\hat{q}}. \quad (15d)$$

Note that, despite their larger size, stiffness matrices of the standard finite element discretization, as they appear in (15b) and (15d), may be assembled much faster than the stiffness matrices $dM_{\hat{\mathcal{S}}}$ and $K_{\hat{\mathcal{Y}}}$ in the formulation given in (14b) and (14d).

4 Implementation Issues

In this section, we address how to compute the measurement matrices by means of standard tools, how to incorporate the initial and terminal values in the time discretization, and how to preassemble quadratic nonlinearities.

4.1 Computation of the Measurements

We explain how the measurements (cf. Remark 2.1) that are needed for the computation of the optimal low-rank bases (cf. Lemma 2.5 and Lemma 2.6) can be obtained in practical cases.

In the standard *method-of-lines* approach, a \mathcal{Y} will be used as the FE space for a Galerkin spatial discretization that approximates (11a) by an ODE. In a second step, a time integration scheme is employed to approximate coefficients $v_1, \dots, v_q: (0, T] \rightarrow \mathbb{R}$ of the solution

$$\bar{v}: (0, T] \rightarrow \mathcal{Y}: t \mapsto \sum_{i=1}^q v_i(t) \nu_i$$

of the resulted ODE. With this and with a chosen time measurement space \mathcal{S} , a numerical computed measurement in $\mathcal{S} \cdot \mathcal{Y}$ of the actual solution v of (11a), is given as

$$\mathbf{X} = \begin{bmatrix} (v_1, \psi_1)_{\mathcal{S}} & \dots & (v_1, \psi_s)_{\mathcal{S}} \\ \vdots & \ddots & \vdots \\ (v_q, \psi_1)_{\mathcal{S}} & \dots & (v_q, \psi_s)_{\mathcal{S}} \end{bmatrix} \mathbf{M}_{\mathcal{S}}^{-1}. \quad (16)$$

Remark 4.1. Since in (16), the matrix \mathbf{X} is computed from a function with values in \mathcal{Y} , the inner products in \mathcal{Y} and the inverse of $\mathbf{M}_{\mathcal{Y}}$ realizing the L^2 -projection onto \mathcal{Y} in (4) are not present.

Remark 4.2. For smooth trajectories and for measurements using delta distributions centered at some $t_j \in (0, T)$, $j = 1, \dots, s$, with $\int_0^T v_i \delta(t_j) dt = v_i(t_j)$ the matrix (16) degenerates to the standard POD *snapshot matrix*. In this case, since the delta distributions are not element of $L^2(0, T)$, there is no way to define an optimal time basis as in Lemma 2.6. However, one can define an optimal low-rank spatial basis by Lemma 2.5 which reduces to the standard POD optimality result with $\mathbf{M}_{\mathcal{S}} = I$, cf. Remark 2.7 and 2.8.

4.2 Treatment of the Initial Value

The initial value (11c) requires a special consideration. Firstly, like the solution of the PDE is only well defined when the initial condition is specified, also the space-time Galerkin discretized system (13) is uniquely solvable if an initial condition is provided. Secondly, in particular in view of optimal control, the initial value can be subject to changes which should be realizable in the discretized model.

To maintain the prominent role of the initial condition also in the time discretization, we proceed as follows:

1. We choose an \mathcal{S} that is spanned by a nodal basis $\{\psi_1, \dots, \psi_s\}$ and that ψ_1 is the basis function associated with the node at $t = 0$.
2. For a given function, we compute \mathbf{X}_0 as in (4) or (16) setting $\psi_1 = 0$ and $U_{\hat{s},0}$ as the matrix of the $\hat{s} - 1$ leading right singular vectors of $\mathbf{L}_y^T \mathbf{X}_0 \mathbf{L}_S$.
3. We set

$$U_{\hat{s}} = \begin{bmatrix} \mathbf{L}_S^T \\ \begin{bmatrix} 1 \\ 0 \\ \vdots \\ 0 \end{bmatrix} \\ U_{\hat{s},0} \end{bmatrix}$$

and compute the reduced basis as in Lemma 2.6 as

$$\begin{bmatrix} \hat{\psi}_1 \\ \hat{\psi}_2 \\ \vdots \\ \hat{\psi}_{\hat{s}} \end{bmatrix} = U_{\hat{s}}^T \mathbf{L}_S^{-1} \begin{bmatrix} \psi_1 \\ \psi_2 \\ \vdots \\ \psi_s \end{bmatrix}.$$

By this construction we obtain that $\hat{\psi}_1 = \psi_1$ will be associated with the initial value, whereas $\hat{\psi}_2(0) = \dots = \hat{\psi}_{\hat{s}}(0) = 0$ will still optimally approximate the trajectory.

4.3 Assembling of Quadratic Nonlinearities

As an example, we consider the nonlinearity in the Burgers' equation

$$\frac{1}{2} \partial_x z(t, x)^2 \tag{17}$$

with the spatial coordinate $x \in (0, 1)$, and the time variable $t \in (0, 1]$.

In the time-space Galerkin projection (12), the il -component of the discretized nonlinearity (14e) in the case of (17), is given as

$$\begin{aligned} H_{il}(\hat{\mathbf{v}}) &= \frac{1}{2} \int_0^1 \int_0^1 \hat{\nu}_i \hat{\psi}_l \cdot \partial_x \hat{v}^2 \, dx \, dt \\ &= \frac{1}{2} \int_0^1 \int_0^1 \hat{\nu}_i \hat{\psi}_l \cdot \partial_x ([\hat{\Psi}^T \otimes \hat{\Upsilon}^T] \hat{\mathbf{v}})^2 \, dx \, dt \\ &= \hat{\mathbf{v}}^T \left[\int_0^1 \hat{\nu}_i \hat{\Psi} \hat{\Psi}^T \, dt \otimes \frac{1}{2} \int_0^1 \hat{\psi}_l \partial_x (\hat{\Upsilon} \hat{\Upsilon}^T)^2 \, dx \right] \hat{\mathbf{v}}, \end{aligned}$$

where we have used the linearity of the *Kronecker product* and that

$$\hat{v}^2 = ([\hat{\Psi}^T \otimes \hat{\Upsilon}^T] \hat{\mathbf{v}})^2 = \hat{\mathbf{v}}^T [\hat{\Psi} \otimes \hat{\Upsilon}] [\hat{\Psi}^T \otimes \hat{\Upsilon}^T] \hat{\mathbf{v}} = \hat{\mathbf{v}}^T [\hat{\Psi} \hat{\Psi}^T \otimes \hat{\Upsilon} \hat{\Upsilon}^T] \hat{\mathbf{v}}.$$

Thus, the evaluation of the discretized nonlinear term can be assisted by precomputing

$$\int_0^1 \hat{\nu}_i \hat{\Psi} \hat{\Psi}^T \, dt \quad \text{and} \quad \frac{1}{2} \int_0^1 \hat{\psi}_l (\hat{\Upsilon} \partial_x \hat{\Upsilon}^T + \partial_x (\hat{\Upsilon} \hat{\Upsilon}^T)) \, dx$$

for all $\hat{\nu}_i, i = 1, \dots, \hat{s}$ and $\hat{\psi}_l, l = 1, \dots, \hat{q}$.

Remark 4.3. If $V_{\hat{q}}$ is the matrix of the spatial POD modes that transform the FEM basis Υ into the reduced basis $\hat{\Upsilon}$ via $\hat{\Upsilon} = V_{\hat{q}}^T \mathbf{L}_y^{-1} \Upsilon$, then the spatial part of the reduced nonlinearity fulfills

$$\begin{aligned} & \frac{1}{2} \int_0^1 \hat{\psi}_l(\hat{\Upsilon} \partial_x \hat{\Upsilon}^T + \partial_x(\hat{\Upsilon}) \hat{\Upsilon}^T) dx = \\ & \frac{1}{2} V_{\hat{q}}^T \mathbf{L}_y^{-1} \int_0^1 \hat{\psi}_l(\Upsilon \partial_x \Upsilon^T + \partial_x(\Upsilon) \Upsilon^T) dx \mathbf{L}_y^{-T} V_{\hat{q}}, \end{aligned}$$

where the inner matrix of the latter expression might be efficiently assembled in a FEM package. The same idea applies to the time-related part.

5 Application in PDE-Constrained Optimization

We consider a generic optimal control problem.

Problem 5.1. *For a given target trajectory $x^* \in L^2(0, T; L^2(\Omega))$ and a penalization parameter $\alpha > 0$, we consider the optimization problem*

$$\mathcal{J}(x, u) := \frac{1}{2} \|x - x^*\|_{L^2}^2 + \frac{\alpha}{2} \|u\|_{L^2}^2 \rightarrow \min_{u \in L^2(0, T; L^2(\Omega))} \quad (18)$$

subject to the generic PDE

$$\dot{x} - \Delta x + N(x) = f + u \quad \text{on } (0, T] \times \Omega, \quad (19a)$$

$$x|_{\partial\Omega} = 0 \quad \text{on } (0, T], \quad (19b)$$

$$x|_{t=0} = x_0 \quad \text{on } \Omega. \quad (19c)$$

If the nonlinearity is smooth, then necessary optimality conditions with respect to Problem 5.1 for (x, u) are given through $u = \frac{1}{\alpha} \lambda$, where λ solves the adjoint equation

$$-\dot{\lambda} - \Delta \lambda + D_x N(x)^T \lambda + x = x^* \quad \text{on } (0, T] \times \Omega, \quad (20a)$$

$$\lambda|_{\partial\Omega} = 0 \quad \text{on } (0, T], \quad (20b)$$

$$\lambda|_{t=T} = 0 \quad \text{on } \Omega, \quad (20c)$$

where D_x denotes the Frechét derivative, which is coupled to the state equation (19) through x and u ; see [17].

Given low-dimensional spaces $\hat{\mathcal{S}} := \text{span}\{\hat{\psi}_1, \dots, \hat{\psi}_{\hat{s}}\}$, $\hat{\mathcal{R}} := \text{span}\{\hat{\phi}_1, \dots, \hat{\phi}_{\hat{r}}\} \subset H^1(0, T)$ and $\hat{\mathcal{Y}} := \text{span}\{\hat{\nu}_1, \dots, \hat{\nu}_{\hat{q}}\}$, $\hat{\mathcal{L}} := \text{span}\{\lambda_1, \dots, \lambda_{\hat{p}}\} \subset H_0^1(\Omega)$, a tensor space-time Galerkin discretization of the coupled system (19)-(20) reads

$$[dM_{\hat{\mathcal{S}}} \otimes M_{\hat{\mathcal{Y}}} + M_{\hat{\mathcal{S}}} \otimes K_{\hat{\mathcal{Y}}}] \hat{\mathbf{v}} + H_{\hat{\mathcal{S}}\hat{\mathcal{Y}}}(\hat{\mathbf{v}}) - \frac{1}{\alpha} [M_{\hat{\mathcal{S}}\hat{\mathcal{R}}} \otimes M_{\hat{\mathcal{Y}}\hat{\mathcal{L}}}] \hat{\boldsymbol{\lambda}} = f_{\hat{\mathcal{S}}\hat{\mathcal{Y}}}, \quad (21a)$$

$$[-dM_{\hat{\mathcal{R}}} \otimes M_{\hat{\mathcal{L}}} + M_{\hat{\mathcal{R}}} \otimes K_{\hat{\mathcal{L}}}] \hat{\boldsymbol{\lambda}} + D_x N_{\hat{\mathcal{L}}\hat{\mathcal{R}}}^T(\hat{\mathbf{v}}) \hat{\boldsymbol{\lambda}} + [M_{\hat{\mathcal{R}}\hat{\mathcal{S}}} \otimes M_{\hat{\mathcal{L}}\hat{\mathcal{Y}}}] \hat{\mathbf{v}} = [M_{\hat{\mathcal{R}}\hat{\mathcal{S}}} \otimes M_{\hat{\mathcal{L}}\hat{\mathcal{Y}}}] \hat{\mathbf{v}}^*, \quad (21b)$$

with the coefficients $dM_{\hat{\mathcal{R}}}$, $M_{\hat{\mathcal{R}}}$, $M_{\hat{\mathcal{L}}}$, $K_{\hat{\mathcal{L}}}$ and the nonlinearity $D_x N_{\hat{\mathcal{L}}\hat{\mathcal{R}}}^T(\hat{\mathbf{v}}) \hat{\boldsymbol{\lambda}}$ defined as in (13), with $M_{\hat{\mathcal{S}}\hat{\mathcal{R}}}$, $M_{\hat{\mathcal{R}}\hat{\mathcal{S}}}$, $M_{\hat{\mathcal{Y}}\hat{\mathcal{L}}}$, $M_{\hat{\mathcal{L}}\hat{\mathcal{Y}}}$ denoting the mixed mass matrices like

$$M_{\hat{\mathcal{S}}\hat{\mathcal{R}}} := [(\hat{\psi}_\ell, \hat{\phi}_k)]_{k=1, \dots, \hat{r}}^{\ell=1, \dots, \hat{s}} \in \mathbb{R}^{\hat{s}, \hat{r}},$$

with $\hat{\mathbf{v}}^*$ representing the target v^* projected onto $\hat{\mathcal{S}} \cdot \hat{\mathcal{Y}}$, with the spatial boundary conditions resolved in the ansatz spaces, and with accounting for the initial and terminal conditions via requiring

$$\hat{v}(0) = \sum_{j=1}^{\hat{q}} \sum_{i=1}^{\hat{s}} \mathbf{x}_{i,j}^1 \hat{\nu}_i \hat{\psi}_j(0) = \Pi_{\hat{\mathcal{Y}}} x_0 \quad \text{and} \quad \hat{\lambda}(T) = \sum_{j=1}^{\hat{r}} \sum_{i=1}^{\hat{p}} \mathbf{x}_{i,j}^1 \hat{\mu}_i \hat{\phi}_j(T) = 0,$$

cf. Chapter 4.2.

6 Numerical Experiments

We consider the optimal control of a Burgers' equation as it was described in [10, 12]. Therefore, in Problem 5.1, we replace the generic PDE (19) by Burgers' equation, namely:

$$\dot{x} - \nu \partial_{\xi\xi} x + \frac{1}{2} \partial_{\xi}(x^2) = u \quad \text{on } (0, T] \times (0, L), \quad (22a)$$

$$x|_{\xi=0, \xi=L} = 0 \quad \text{on } (0, T], \quad (22b)$$

$$x|_{t=0} = x_0 \quad \text{on } (0, L), \quad (22c)$$

where L and T denote the length of the space and time interval and where $\nu > 0$ is a parameter. We set $T = 1$ and $L = 1$ and, as the initial value, we take the step function

$$x_0: (0, 1) \rightarrow \mathbb{R}: \xi \mapsto \begin{cases} 1, & \text{if } \xi \leq 0.5 \\ 0, & \text{if } \xi > 0.5 \end{cases}. \quad (23)$$

As for the target, we define x^* via $x^*(t) = x_0$, which means that the optimization is designed to keep the system in its initial state.

Thus the concrete problem reads as follows:

Problem 6.1. *Given parameters ν and α , find $u \in L^2(0, 1; L^2(0, 1))$ such that*

$$\frac{1}{2} \int_0^1 \int_0^1 (x(t, \xi) - x_0)^2 \, d\xi \, dt + \frac{\alpha}{2} \int_0^1 \int_0^1 u^2(t, \xi) \, d\xi \, dt \rightarrow \min_{u \in L^2(0, 1; L^2(0, 1))} \quad (24)$$

subject to Burgers' equation (22).

6.1 Space-time Generalized POD for Optimal Control

The general procedure is as follows:

1. Do at least one forward solve of the state equation (22) and at least one backward solve of the adjoint equation (20) to setup generalized measurement matrices of the state and the costate as explained in Section 4.1.
2. Compute optimized space and time bases for the state and the costate as defined in Lemma 2.5 and 2.6. To account for the initial and the terminal value, one may resort to the procedure explained in Section 4.2.
3. Set up the projected closed-loop optimality system (21) and solve for the optimal costate $\hat{\lambda}$ of the reduced system.
4. Lift $\hat{u} = \frac{1}{\alpha} \hat{\lambda}$ up to the full space-time grid and apply it as suboptimal control to the actual problem.

The procedure is defined by several parameters. In the presented examples, we fix $\mathcal{Y} = \Lambda$ and $\mathcal{S} = \mathcal{R}$, corresponding to the initial space and time discretizations, and investigate the influence of the other parameters on the numerical solution of the optimal control problem. See Table 1 for an overview of the parameters and their default values.

We will measure the performance of the approach through:

- The time `walltime` it takes to solve the reduced optimality system (21) for $\hat{\lambda}$, reporting the best number out of 5 runs.
- The difference $\|\hat{x} - x_0\|_{L^2}$ between the target state and the state \hat{x} achieved by using the suboptimal control \hat{u} on the base of $\hat{\lambda}$ in the simulation of the full model.
- The value $\mathcal{J}(\hat{x}, \hat{u})$ of the cost function (24).

Parameter	Description	Base Value	Range
\mathcal{Y}, Λ	Space of piecewise linear finite elements on an equidistant grid of dimension q, p	$q = p = 220$	–
\mathcal{S}, \mathcal{R}	Space of linear hat functions on an equidistant grid of dimension s, r	$s = r = 120$	–
$\hat{\mathcal{Y}}, \hat{\Lambda}$	POD reductions of \mathcal{Y} and Λ of dimension \hat{q}, \hat{p} ; cf. Lemma 2.5	$\hat{q} = \hat{p} = 12$	6 – 24
$\hat{\mathcal{S}}, \hat{\mathcal{R}}$	POD reductions of \mathcal{S} and \mathcal{R} of dimension \hat{s}, \hat{r} ; cf. Lemma 2.6	$\hat{r} = \hat{s} = 12$	6 – 24
α	Regularization parameter in the cost functional (24)	$1 \cdot 10^{-3}$	$2.5 \cdot 10^{-4} - 1.6 \cdot 10^{-2}$
ν	Viscosity parameter in the PDE (22)	$2 \cdot 10^{-3}$	$5 \cdot 10^{-4} - 1.6 \cdot 10^{-2}$

Table 1: Description and values of the parameters of the numerical examples of Section 6.1

The spatial discretization is carried out with the help of the FEM library *FEniCS* [13]. For the time integration, we use *SciPy*'s builtin ODE-integrator `scipy.integrate.odeint`. To solve the nonlinear system (21) for $\hat{\lambda}$, we use *SciPy*'s routine `scipy.optimize.fsolve`. The norms are approximated in the used FEM space. The implementation and the code for all tests as well as the documentation of the hardware are available from the author's public git repository [9]; see also the section on code availability on page 16.

Choice of the measurements. The computation of the measurements and the choice of the reduced bases is an important parameter of the approach. Generally the basis of $\hat{\mathcal{S}} \cdot \hat{\mathcal{Y}}$ should be well suited to approximate the state, whereas the basis $\hat{\mathcal{R}} \cdot \hat{\Lambda}$ should well represent the adjoint state. In the optimization case, where the suboptimal input is defined through $\frac{1}{\alpha} \hat{\lambda}$ and its lifting to the full-order space, two other conditions emerge. Firstly, the reduced basis of the adjoint state, should also well approximate the optimal control. Secondly, the bases of the state and the adjoint must not be orthogonal or “almost” orthogonal such that the joint mass matrix $[M_{\hat{\mathcal{S}}\hat{\mathcal{R}}} \otimes M_{\hat{\mathcal{Y}}\hat{\Lambda}}]$ degenerates and the contribution of the input in (21a) vanishes.

As illustrated in the plots in Figure 1, the straight-forward approach of constructing the bases for the state by means of state measurements and the basis for the adjoint by means of measurements of the adjoint, well approximates the state and the adjoint but not the closed-loop problem. It turned out that taking the state measurements to also construct the reduced space for the adjoint gave a better approximation to the optimality system while, naturally, only poorly approximating the adjoint. The best result were obtained in combining state and adjoint state measurements to construct the bases.

Thus, for the computation of the optimal bases for the following tests, we combined the measurements obtained from one forward solve with no control and one backward solve with the state from the forward solve and the target state.

Overall Number of Modes. In these tests we examine how the number of modes, i.e. the dimension of the reduced order system, affects the time needed to solve the reduced order system and the value of the cost functional (24) achieved through the suboptimal control.

We fix $\nu = 0.005$ and set $\hat{q} = \hat{p} = \hat{r} = \hat{s} = \hat{K}/4$, with $\hat{K} \in \{24, 36, 48, 72, 96\}$. Thus, for every setup, the nonlinear system (21) of dimension \hat{K} has to be solved for the optimal costate $\hat{\lambda}$. The results of these tests are reported in Table 2.

As expected, the larger the reduced model, the lower the achieved values of the cost functional. Also, with growing order of the reduced model, the time needed to solve the corresponding nonlinear system increases drastically.

Space vs. Time Reduction From the previous tests, we found that in the considered setup, an overall number of $\hat{K} = 48$ modes is a good compromise between accuracy and computation time. In this section, we examine how the distribution of modes between space and time affects the quality of the suboptimal control. Therefore, and for a varying

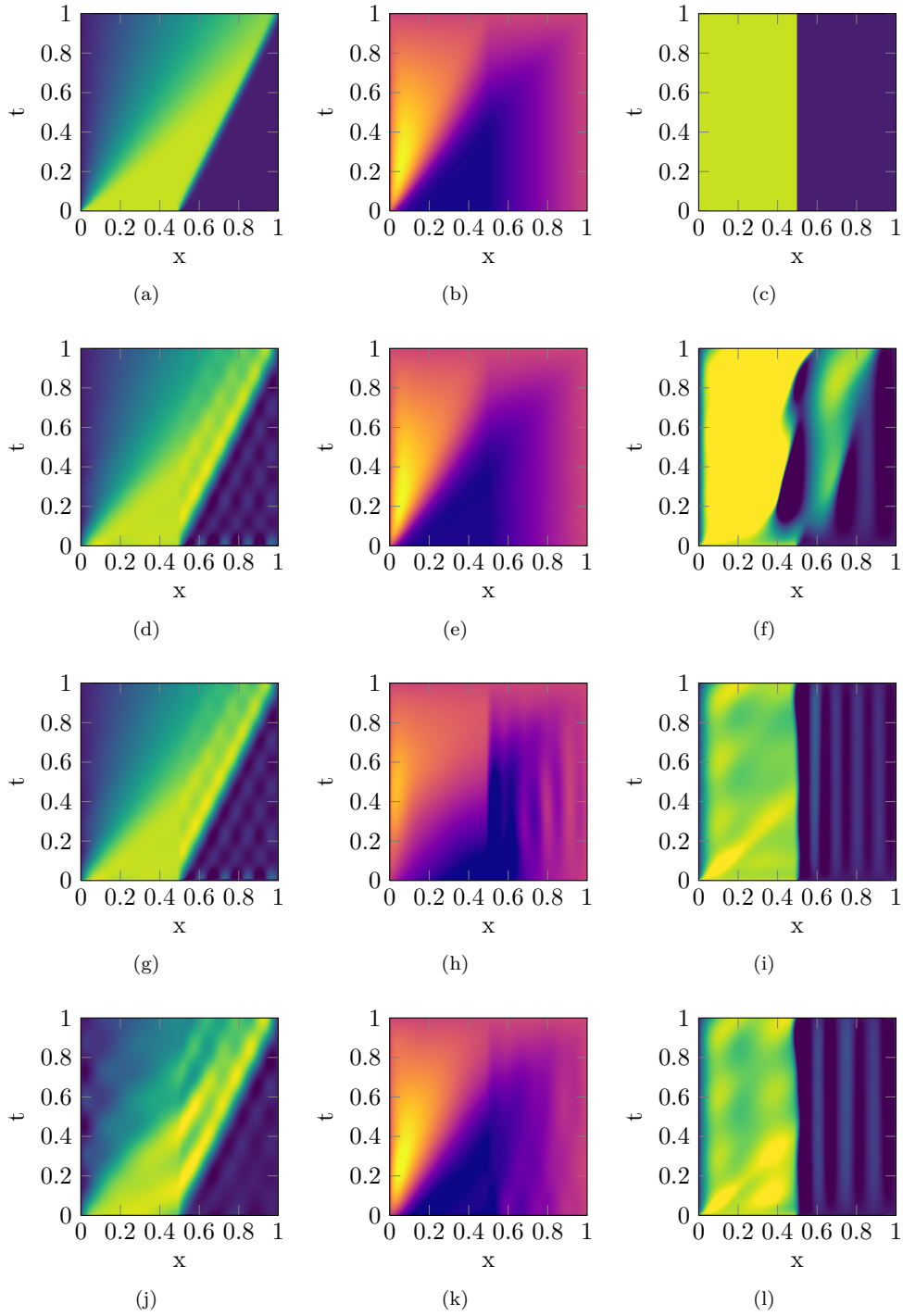


Figure 1: Illustration of the effect of the choice of the snapshots on the performance of the low-dimensional approximations of the state (a), the adjoint state (b), and on how outcome of the optimization matches the target state (c). The second row (d-f) corresponds to the case that snapshots of the state and the adjoint are used to approximate the state and the adjoint, respectively. For the results depicted in the third row (g-i), the optimized basis for the state was used also for the adjoint. The results depicted in the last row (j-l) were obtained by combining state and adjoint snapshots for the computation of the reduced bases. For a comparable illustration we have used color maps with linear intensity on the intervals $[-0.1, 1.1]$ for the states and $[-0.5, 0.5]$ for the adjoint states. Values that exceeded these margins were cropped.

increment/decrement j , we set $\hat{q} = \hat{p} := 12 \mp j$ and $\hat{s} = \hat{r} := 12 \pm j$. Accordingly, the overall number of degrees of freedom stays constant throughout the tests but we add weight on the approximation of either the time or the space component.

The results are listed in Table 3. It turns out that up to a certain level, it is beneficial to emphasize on the space as opposed to the time resolution. In the considered setup, the distribution of 16 degrees of freedom in space versus 8 in time gave the best results in terms of performance of the corresponding suboptimal control. Interestingly, also the timings `walltime` vary significantly. This variance is due to different convergence behavior of the optimization algorithm used to solve the nonlinear system.

Reduced Order Model vs. Viscosity Parameter In these tests, we examine how the low-rank space-time Galerkin approach performs over a range of viscosity parameters ν . It is known that for low values of ν , the problem is *convection dominated* and hard to approximate by POD bases. In the considered setup, where the target state is a nonsmooth function, we also expect a decreasing performance for larger values of ν , since the diffusion makes the step in the target untrackable.

The results are listed in Table 4 for $(\hat{q}, \hat{s}) = (\hat{p}, \hat{r}) = (16, 8)$, which was the optimal distribution as found in the previous tests, and in Table 5 for $(\hat{q}, \hat{s}) = (\hat{p}, \hat{r}) = (12, 12)$. The optimal distribution $(16, 8)$ has its performance peak at $\nu = 8 \cdot 10^{-3}$. It also shows the expected pattern that for lower values of ν , for which the nonlinearity gets more emphasis, the time for the solution of the nonlinear system increases. The results of the runs with equally distributed numbers of space and time modes $(12, 12)$ are listed in Table 5. The comparison to the distribution $(16, 8)$ does not give a clear conclusion. For higher viscosities the $(12, 12)$ -case is worse in all categories. For low viscosities, it outperforms the $(16, 8)$ case in terms of computation time and, for the lowest investigated value of ν , even in terms of approximation quality.

Regularization Parameter In this section, we examine the influence of the regularization parameter α onto the performance. Therefore we fix $\nu = 5 \cdot 10^{-3}$, $(\hat{q}, \hat{s}) = (\hat{p}, \hat{r}) \in \{(16, 8), (12, 12)\}$, and vary α which defines the penalization of the control magnitude in the cost functional (24).

The results are listed in Table 6 for the $(16, 8)$ -case and in Table 7 for the $(12, 12)$ -case. For higher values of α , for both cases, the optimization performs similarly well in approximating the control problem, with a clear advantage of the $(16, 8)$ distribution in terms of computation time. For lower values of α the $(16, 8)$ setup outperforms the $(12, 12)$ by far. Interestingly, for the smallest α , the tracking error $\frac{1}{2} \|\hat{x} - x_0\|_{L^2}^2$ increases again.

6.2 Gradient-based Classical POD-reduced Optimal Control

In this section we consider the suboptimal numerical solution of Problem 6.1 based on a (spatial) POD reduction in a classical *method-of-lines* approach, cf. [12]. After finite element discretization in space, we consider (22) in semi-discretized form,

$$M_Y \partial_t \mathbf{x}(t) + \nu K_Y \mathbf{x}(t) + H_Y(\mathbf{x}) - M_\Lambda \mathbf{u}(t) = \mathbf{0}, \quad (25a)$$

$$\mathbf{x}(0) = \mathbf{x}_0, \quad (25b)$$

where mass and stiffness matrices are defined in the same way as their reduced-order counterparts in (14a)-(14f). Classical POD is based on an SVD of the so-called snapshot matrix taken from s distinct time instances,

$$X = [\mathbf{x}(t_1), \dots, \mathbf{x}(t_s)] \in \mathbb{R}^{q \times s}. \quad (26)$$

For $U_{\hat{q}}$ being the matrix that consists of the \hat{q} leading left singular vectors of (26), we introduce the reduced state variable via $\mathbf{x}(t) \approx U_{\hat{q}} \hat{\mathbf{x}}(t)$. Similarly, a reduced-order control variable $\hat{\mathbf{u}}$ can be introduced. A suboptimal solution to Problem 6.1 can be obtained by

\hat{K}	24	36	48	72	96
$\frac{1}{2}\ \hat{x} - x_0\ _{L^2}^2$	0.0330	0.0280	0.0192	0.0121	0.0104
$\mathcal{J}(\hat{x}, \hat{u})$	0.0351	0.0309	0.0234	0.0177	0.0152
walltime [s]	0.1	0.48	1.81	18.7	155

Table 2: Performance of the suboptimal control versus varying resolutions of space and time.

$(\hat{q}, \hat{s})/(\hat{p}, \hat{r})$	(18, 6)	(17, 7)	(16, 8)	(14, 10)	(12, 12)	(10, 14)	(8, 16)
$\frac{1}{2}\ \hat{x} - x_0\ _{L^2}^2$	0.0138	0.0125	0.0117	0.0137	0.0192	0.0326	0.0339
$\mathcal{J}(\hat{x}, \hat{u})$	0.0184	0.0173	0.0167	0.0184	0.0234	0.0364	0.0364
walltime	0.98	1.84	1.19	1.57	1.81	1.49	1

Table 3: Performance of the suboptimal control versus varying distributions of space and time resolutions.

ν	$5 \cdot 10^{-4}$	$1 \cdot 10^{-3}$	$2 \cdot 10^{-3}$	$4 \cdot 10^{-3}$	$8 \cdot 10^{-3}$	$1.6 \cdot 10^{-2}$	$3.2 \cdot 10^{-2}$
$\frac{1}{2}\ \hat{x} - x_0\ _{L^2}^2$	1.1072	0.1368	0.0188	0.0126	0.0098	0.0111	0.0198
$\mathcal{J}(\hat{x}, \hat{u})$	1.8489	0.1994	0.0225	0.0173	0.0150	0.0168	0.0268
walltime	2.95	7.13	1.91	1.04	1.07	1	1.64

Table 4: Performance of the suboptimal control versus varying diffusion parameters ν for $(\hat{q}, \hat{s}) = (\hat{p}, \hat{r}) = (16, 8)$.

ν	$5 \cdot 10^{-4}$	$1 \cdot 10^{-3}$	$2 \cdot 10^{-3}$	$4 \cdot 10^{-3}$	$8 \cdot 10^{-3}$	$1.6 \cdot 10^{-2}$	$3.2 \cdot 10^{-2}$
$\frac{1}{2}\ \hat{x} - x_0\ _{L^2}^2$	0.0236	0.0259	0.0263	0.0217	0.0153	0.0123	0.0210
$\mathcal{J}(\hat{x}, \hat{u})$	0.0269	0.0293	0.0299	0.0256	0.0201	0.0176	0.0281
walltime	1.60	2.06	1.76	1.24	1.64	1.8	1.9

Table 5: Performance of the suboptimal control versus varying diffusion parameters ν for $(\hat{q}, \hat{s}) = (\hat{p}, \hat{r}) = (12, 12)$.

α	$2.5 \cdot 10^{-4}$	$5 \cdot 10^{-4}$	$1 \cdot 10^{-3}$	$2 \cdot 10^{-3}$	$4 \cdot 10^{-3}$	$8 \cdot 10^{-3}$	$1.6 \cdot 10^{-2}$
$\frac{1}{2}\ \hat{x} - x_0\ _{L^2}^2$	0.0137	0.0121	0.0117	0.0124	0.0144	0.0179	0.0237
$\mathcal{J}(\hat{x}, \hat{u})$	0.0158	0.0155	0.0167	0.0196	0.0240	0.0305	0.0398
walltime	1.12	0.96	1.18	1.4	1.59	1.82	1.88

Table 6: Performance of the suboptimal control versus varying regularization parameters α for $(\hat{q}, \hat{s}) = (\hat{p}, \hat{r}) = (16, 8)$.

α	$2.5 \cdot 10^{-4}$	$5 \cdot 10^{-4}$	$1 \cdot 10^{-3}$	$2 \cdot 10^{-3}$	$4 \cdot 10^{-3}$	$8 \cdot 10^{-3}$	$1.6 \cdot 10^{-2}$
$\frac{1}{2}\ \hat{x} - x_0\ _{L^2}^2$	0.0488	0.0293	0.0192	0.0148	0.0145	0.0168	0.0215
$\mathcal{J}(\hat{x}, \hat{u})$	0.0504	0.0318	0.0234	0.0213	0.0239	0.0301	0.0393
walltime	1.31	1.59	1.81	1.97	2.02	2.5	3.73

Table 7: Performance of the suboptimal control versus varying regularization parameters α for $(\hat{q}, \hat{s}) = (\hat{p}, \hat{r}) = (12, 12)$.

minimizing the corresponding fully discretized POD-reduced Lagrangian function,

$$\begin{aligned} & \hat{\mathcal{L}}(\hat{\mathbf{x}}_0, \dots, \hat{\mathbf{x}}_{n_t}, \hat{\mathbf{u}}_0, \dots, \hat{\mathbf{u}}_{n_t}, \hat{\boldsymbol{\lambda}}_1, \dots, \hat{\boldsymbol{\lambda}}_{n_t}) \\ &= \sum_{j=0}^{n_t} \delta t \left(\frac{1}{2} \hat{\mathbf{x}}_j^\top M_{\mathcal{Y}} \hat{\mathbf{x}}_j - (\hat{\mathbf{x}}_j^*)^\top \hat{\mathbf{x}}_j + \frac{\alpha}{2} \hat{\mathbf{u}}_j^\top M_{\hat{\Lambda}} \hat{\mathbf{u}}_j \right) \\ &+ \sum_{j=0}^{n_t-1} \hat{\boldsymbol{\lambda}}_{j+1}^\top \left[M_{\mathcal{Y}} \left(\frac{\hat{\mathbf{x}}_{j+1} - \hat{\mathbf{x}}_j}{\delta t} \right) + \nu K_{\mathcal{Y}} \hat{\mathbf{x}}_{j+1} + H_{\mathcal{Y}}(U_{\hat{q}} \hat{\mathbf{x}}_{j+1}) - M_{\hat{\Lambda}} \hat{\mathbf{u}}_{j+1} \right], \end{aligned} \quad (27)$$

where we refer the reader to [2, 10] for a detailed derivation. In the following numerical experiments, we use n_t time steps for an implicit Euler time integration, and use a gradient-based optimization scheme for minimizing (27). The gradient $\nabla_{\hat{\mathbf{u}}} \hat{\mathcal{L}}$ is computed using the adjoint approach of [10, Algorithm 6.1] which is solved *backwards in time*. To compare with the results in Section 6.1 as best as possible, we use the same base parameters, namely $s = 120$ equidistantly distributed snapshots in (26), and a linear finite element basis of dimension $q = 220$ for the spatial component of the full-order model (25). In Table 2, we use the BFGS implementation [15] with a stopping criterion that targets the objective function values achieved in Table 2. When $\hat{q} = n_t$ are increased, we observe that the objective function value improves at a linear cost. These results can be improved when DEIM [7] at a fixed dimension of 25 DEIM points is used to approximate the nonlinear term in (27). A comparison with the gradient-based SPG method [5] is given in [2] and yields similar results.

In a second experiment we mimic the experiments reported in Table 3. Therefore, we vary the ratio of POD dimension \hat{p} versus number of Euler time integration steps n_t . Also here, the best results are obtained when the spatial dimension is large compared to the time discretization.

In the previous two experiments, BFGS was terminated based on a priori knowledge. In Table 10, we chose a stopping criterion based on a tolerance for the gradient of the Lagrangian (27). The timings presented in Table 10 are for the case $\hat{q} = n_t = 18$ and indicate that the configuration used in Table 8 is close to optimal.

7 Conclusion and Outlook

We have presented a novel approach to low-rank space-time Galerkin approximations that bases on a generalization of classical snapshot-based POD which then can be extended to POD reduction of time discretizations. We have proved optimality of the reduced bases in the relevant function spaces and discussed the numerical implementation.

The space-time Galerkin POD reduction applies well to optimal control problems, as we have illustrated it for the optimal control of a Burgers' equation. Both in terms of computation time for and efficiency of a suboptimal control, the new approach can compete with the combination of classical POD/DEIM for model reduction and BFGS for the optimization. For an optimized distribution of space and time modes, our new approach even dominates the POD/BFGS implementation by achieving better accuracy in less time.

One major potential of the new low-rank space-time Galerkin approach to optimization problems is that it solves the boundary value problem in one shot rather than decoupling forward and backward time like all gradient-based methods do.

Further possible improvements and issues to future work concerning the proposed space-time POD in application to optimal control problems lie in the freedom of the choice of the measurement functions [4]. Moreover, the underlying tensor structure is readily extended to include further directions of the state space like parameter dependencies [3] or inputs. Another issue that needs to be addressed is the treatment of general nonlinearities that can not be treated by preassembling like in the presented quadratic case. Then, an inclusion of *empirical interpolation* (EIM) [1] might be needed to achieve efficiency of the reduction. Moreover, it seems worth investigating whether the principles of space-time POD can be used to construct optimized bases for the interpolation.

Code Availability

The source code of the implementations used to compute the presented results can be obtained from:

doi:10.5281/zenodo.166339

and is authored by: Manuel Baumann and Jan Heiland
Please contact Manuel Baumann and Jan Heiland for licensing information

Acknowledgements

We thank Joost van Zwieten, co-developer of *Nutils*¹, for providing benchmarks and valuable insight into space-time discretizations of Burgers' equation.

References

- [1] M. Barrault, Y. Maday, N. C. Nguyen, and A. T. Patera. An ‘empirical interpolation’ method: application to efficient reduced-basis discretization of partial differential equations. *C. R. Math. Acad. Sci. Paris*, 339(9):667–672, 2004.
- [2] M. Baumann. Nonlinear model order reduction using pod/deim for optimal control of burgers’ equation. Master’s thesis, Delft University of Technology, 2013.
- [3] M. Baumann, P. Benner, and J. Heiland. A generalized POD space-time Galerkin scheme for parameter dependent dynamical systems. Poster at the MoRePaS III - Workshop on "Model Reduction for Parametrized Systems", published in ScienceOpen Posters, 2015. doi:10.14293/P2199-8442.1.SOP-MATH.P8ECXQ.v1.
- [4] M. Baumann, J. Heiland, and M. Schmidt. Discrete input/output maps and their relation to Proper Orthogonal Decomposition. In P. Benner, M. Bollhöfer, D. Kressner, C. Mehl, and T. Stykel, editors, *Numerical Algebra, Matrix Theory, Differential-Algebraic Equations and Control Theory*, pages 585–608. Springer International Publishing, 2015.
- [5] E. G. Birgin, J. M. Martinez, and M. Raydan. Nonmonotone spectral projected gradient methods on convex sets. *SIAM J. Optim.*, 10:1196–1211, 2000.
- [6] K. Carlberg, J. Ray, and B. van Bloemen Waanders. Decreasing the temporal complexity for nonlinear, implicit reduced-order models by forecasting. *Comp. Meth. Appl. Mech. Eng.*, 289:79–103, 2015.
- [7] S. Chaturantabut and D. Sorensen. Nonlinear Model Reduction via Discrete Empirical Interpolation. *SIAM J. Sci. Comput.*, 32:2737–2764, 2010.
- [8] F. Chinesta, A. Ammar, A. Leygue, and R. Keunings. An overview of the proper generalized decomposition with applications in computational rheology. *J. Non-Newtonian Fluid Mech.*, 166(11):578–592, 2011.
- [9] J. Heiland. spacetime-genpod-burgers – Python module for space-time-parameter generalized POD for Burgers equation. <https://gitlab.mpi-magdeburg.mpg.de/heiland/spacetime-genpod-burgers>, 2015.
- [10] M. Heinkenschloss. Numerical solution of implicitly constrained optimization problems. Technical report, Department of Computational and Applied Mathematics, Rice University, 2008.

¹Open source finite element toolbox for Python: <http://nutils.org>

- [11] B. N. Khoromskij and C. Schwab. Tensor-structured Galerkin approximation of parametric and stochastic elliptic PDEs. *SIAM J. Sci. Comput.*, 33(1):364–385, 2011.
- [12] K. Kunisch and S. Volkwein. Control of the Burgers Equation by a Reduced-Order Approach Using Proper Orthogonal Decomposition. *Journal of Optimization Theory and Applications*, 102(2):345–371, 1999.
- [13] A. Logg, K. B. Ølgaard, M. E. Rognes, and G. N. Wells. FFC: the FEniCS form compiler. In *Automated Solution of Differential Equations by the Finite Element Method*, pages 227–238. Springer, Berlin, Germany, 2012.
- [14] S. Murman, L. Diosady, A. Garai, and M. Ceze. A space-time Discontinuous-Galerkin approach for separated flows. Technical report, AIAA Paper 2016-1059, 2016.
- [15] H. B. Nielsen. IMMOPTIBOX. A Matlab toolbox for optimization and data fitting. Informatics and Mathematical Modelling, Technical University of Denmark, DTU, 2005. <http://www.imm.dtu.dk/~hbn/immoptibox>.
- [16] C. Schwab and R. Stevenson. Space-time adaptive wavelet methods for parabolic evolution problems. *Math. Comp.*, 78(267):1293–1318, 2009.
- [17] F. Tröltzsch. *Optimale Steuerung partieller Differentialgleichungen*. Vieweg+Teubner, Wiesbaden, Germany, 2009.
- [18] J. Van Zwieten, R. A. Henkes, D. R. Van Der Heul, P. I. Rosen Esquivel, B. Sanderse, and C. Vuik. Space-time hp-adaptive DG-FEM schemes for one-dimensional multiphase flow models. In *10th International Conference on CFD in Oil & Gas, Metallurgical and Process Industries*, pages 491–500, 2014.
- [19] S. Volkwein. *Model reduction using proper orthogonal decomposition*. Lecture Notes, Institute of Mathematics and Scientific Computing, University of Graz, 2011.
- [20] S. Volkwein and S. Weiland. An algorithm for Galerkin projections in both time and spatial coordinates. *Proc. 17th MTNS*, 2006.
- [21] M. Yano, A. T. Patera, and K. Urban. A space-time hp-interpolation-based certified reduced basis method for Burgers’ equation. *Math. Models Methods Appl. Sci.*, 24(09):1903–1935, 2014.

$\hat{q} = n_t$	POD					POD-DEIM				
	6	9	12	18	24	6	9	12	18	24
$\frac{1}{2}\ \hat{x} - x_0\ _{L^2}^2$	0.0355	0.0306	0.0216	0.0130	0.0131	0.0353	0.0305	0.0223	0.0157	0.0103
$\mathcal{J}(\hat{x}, \hat{u})$	0.0363	0.0318	0.0240	0.0178	0.0175	0.0356	0.0310	0.0234	0.0182	0.0153
#BFGS	45	62	93	134	203	30	47	77	117	168
walltime	0.20	0.41	0.80	1.78	3.80	0.13	0.28	0.60	1.43	2.81

Table 8: Performance of suboptimal control based on a classical spatial POD and POD-DEIM reduction for the state and control variable. BFGS is terminated based on targeting the suboptimal value of $\mathcal{J}(\hat{x}, \hat{u})$ in Table 2. We fix $\nu = 0.005$ and $\alpha = 0.001$.

(\hat{q}, n_t)	(18, 6)	(17, 7)	(16, 8)	(14, 10)	(12, 12)	(10, 14)	(8, 16)
$\frac{1}{2}\ \hat{x} - x_0\ _{L^2}^2$	0.0217	0.0216	0.0209	0.0218	0.0216	0.0205	0.0184
$\mathcal{J}(\hat{x}, \hat{u})$	0.0238	0.0236	0.0236	0.0237	0.0240	0.0236	0.0235
#BFGS	70	72	85	84	93	95	111
walltime	0.37	0.43	0.55	0.66	0.80	0.88	1.10

Table 9: Performance of the POD-Lagrangian suboptimal control for varying spatial POD reduction and temporal integration.

tol_{∇}	1e-2	5e-3	1e-3	5e-4	1e-4	5e-5	1e-5
$\mathcal{J}(\hat{x}, \hat{u})$	0.0738	0.0738	0.0487	0.0487	0.0173	0.0163	0.0162
#BFGS	7	7	23	23	138	186	259
walltime	0.10	0.11	0.32	0.32	1.83	2.38	3.14

Table 10: Performance of POD-Lagrangian suboptimal control for $\hat{q} = n_t = 18$. BFGS is stopped when $\|\nabla_{\hat{u}}\hat{\mathcal{L}}\|_{\infty} \leq \text{tol}_{\nabla}$, as provided in [15].